

Electronics Upgrade of the Run II DØ Calorimeter and its Performance

Shaohua Fu (on behalf of the DØ Collaboration)

Abstract—The front-end electronics of the DØ Ur/liquid argon calorimeter has been replaced to operate with the new shorter time separation between particle bunches at the Run II of the Fermilab Tevatron. The upgrades of the electronic readout system are described, and the first results of the calibration and the performance of the calorimeter are presented.

I. INTRODUCTION

THE Tevatron accelerator complex at Fermilab has been upgraded after Run I (1992-1996). The center-of-mass energy of collision has been increased from 1.8 TeV to 1.96 TeV. The major upgrades include the construction of the Main Injector and the Antiproton Recycler, within a common tunnel. The plan is to deliver an integrated luminosity of 4.4 fb^{-1} as the base projection and 8.6 fb^{-1} as the design projection by the end of FY2009 (Run I delivered luminosity is about 125 pb^{-1}). At the time of the conference, the luminosity recorded at DØ is about 200 pb^{-1} . The higher instantaneous luminosity requires a reduction in the time separation between particle bunches from the Run I value of $3.56 \mu\text{s}$ to 396 ns in Run II.

The upgrade of the DØ detector is designed to enhance its capabilities from Run I and to accommodate the shorter bunch spacing time. Since the start of the Tevatron Run II in March 2001, the upgraded DØ detector is in operation. In the following we will briefly overview major upgrades of the DØ detector and then discuss the upgrades for calorimeter in details.

II. DØ DETECTOR UPGRADE

Fig. 1 depicts the overview of the upgraded DØ detector. From inside to outside are the three primary detector systems: inner tracking, calorimeter and muon systems. The inner tracking system has been completely replaced with a Silicon Microstrip Tracker (SMT) closest to the beampipe, and a multi-layered scintillating Central Fiber Tracker (CFT) outside of it. The new tracking system sits inside a 2 Tesla magnetic field provided by a new 2.7 m long superconducting solenoid for momentum measurement of charged particles.

The calorimeter, divided into a Central Calorimeter (CC) and two End-cap Calorimeters (EC), has been kept in place, with a replacement of the readout electronics and the online calibration system. A scintillator based central preshower detector with wavelength shifting fiber readout is added between the outer radius of the solenoid and the inner radius of the central calorimeter cryostat to provide electron identification and to compensate for energy loss in the solenoid. In the forward region, a preshower detector similar to the central one is installed on the faces of the endcap calorimeter cryostats. At a larger radius on the inner surface of each EC cryostat, the photo multiplier tubes used for the scintillator based Inter-cryostat Detector (ICD) have been relocated to a region of lower magnetic field, to cover the gap between the CC and EC calorimeters. New scintillator based muon trigger detectors covering the full pseudorapidity range have been added to provide a fast trigger. In the forward muon system, the proportional drift tubes have been replaced with planes of plastic mini-drift tubes.

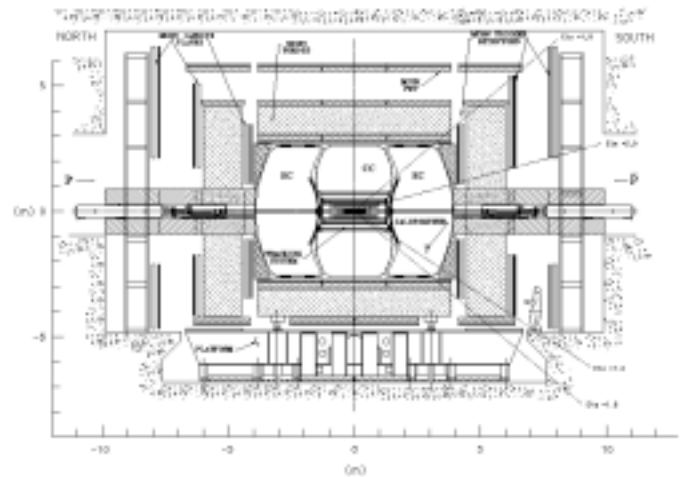


Fig. 1. Side view of the DØ upgraded detector in Run II.

A new 3-level trigger system and data acquisition system are used to handle the high event rate and to provide pipelining of the front-end signals from the tracking, calorimeter, and muon systems. The Level 1 (L1) trigger provides a fast decision on whether to keep or discard an event based on fast detector pick-offs and reduces the input rate to 1.4 kHz. L1 trigger decision time is $4.2 \mu\text{s}$ and it is effectively deadtimeless. The Level 2 trigger consists of dedicated processors that can make

Manuscript received October 18, 2003.

S. Fu is with the Columbia University group at the DØ Experiment, Fermi National Accelerator Laboratory, Batavia, IL 60510 USA (telephone: 630-840-8757, e-mail: shfu@fnal.gov).

the decision in 100 μ s and further reduce the rate to 800 Hz. The Level 3 trigger consists of a farm of commercial processors that utilize fully digitized information to reduce the accept rate to 50 Hz.

III. THE CALORIMETER

The $D\phi$ uranium/liquid argon sampling calorimeter has been described in details in [1]-[2], and is unchanged for Run II. In this section we briefly summarize the important features of the calorimeter. As shown in Fig. 2, the calorimeter consists of three liquid argon cryostats – one Central Calorimeter (CC) covering the region $|\eta| < 1.2$, and two End-cap Calorimeters (EC) extending the coverage to $|\eta| \approx 4$. The Inter-cryostat Detector (ICD) covers the overlapping region $1.1 < |\eta| < 1.4$ between CC and EC.

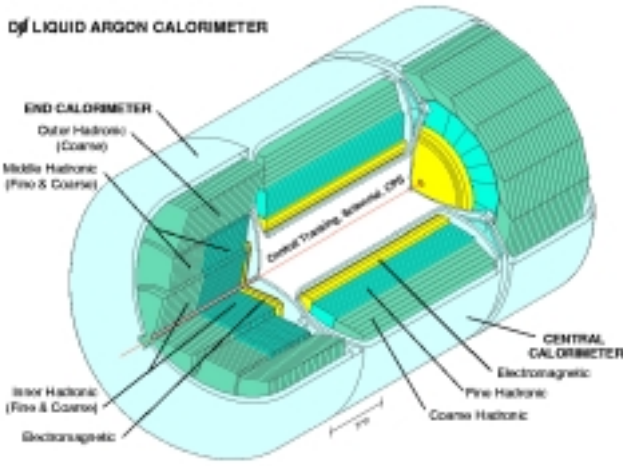


Fig. 2. The $D\phi$ calorimeter.

The calorimeter is highly modular and finely segmented in the transverse and longitudinal shower directions. Three distinct types of modules are used in the CC and EC: an electromagnetic section (EM) with relatively thin and closely spaced uranium absorber plates, a fine hadronic section (FH) with thicker and widely spaced uranium plates and a coarse hadronic section (CH) with thick copper or stainless steel plates. Each module consists of a row of interleaved absorber plates and signal readout boards, as shown in Fig. 3. The 2.3 mm gap separating adjacent absorber plates and signal boards is filled with liquid argon as the active medium. The signal boards are constructed by laminating a copper pad with two separate 0.5 mm thick G10 sheets at each end. The outer surfaces of the boards are coated with a highly resistive epoxy. An electric field is established by grounding the absorber plates while applying a positive potential of 2.0 kV to the resistive surfaces of the signal boards. The electron drift time in the liquid argon gap is about 430 ns, which sets the time scale for signal charge collection. Signals from several signal boards at approximately the same η and ϕ are ganged together in depth to form a readout cell. The readout layers are arranged

into pseudo-projective towers of size 0.1×0.1 in $\Delta\eta \times \Delta\phi$. A projective tower consists of 8-12 layers. To capture the profile of electromagnetic showers, the third layer of the EM section, which corresponds to the shower maximum, is segmented more finely transversely into 0.05×0.05 in $\Delta\eta \times \Delta\phi$.

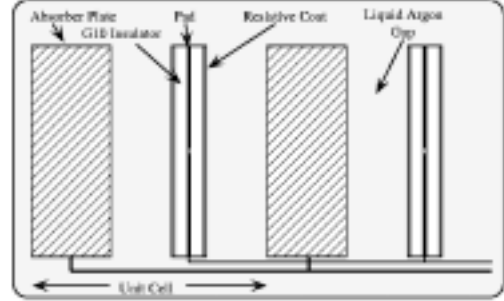


Fig. 3. Schematic view of a calorimeter cell.

A. The Inter-cryostat Detector

In the intermediate region of the calorimeter ($1.1 < |\eta| < 1.4$), the rapidly changing material profile and extra un-instrumented material lead to reduced sampling of showers and hence a degradation of energy measurements in this region. The Inter-cryostat Detector (ICD) [3] restores energy resolution by providing additional sampling in this region, which improves the jet energy and missing energy measurements. The ICD consists of 16 supertiles per EC-region for a total of 378 scintillator tiles (one of the supertile is only half in size and has 6 tiles), as shown in Fig. 4. The tile segmentation of 0.1×0.1 in $\Delta\eta \times \Delta\phi$ matches that of the calorimeter projective towers. The scintillators are read out by photomultiplier tubes (PMT) via wavelength shifting fibers (WLS). The original Run I PMTs are reused but moved to a region of reduced magnetic field, with 5-6 m long clear fiber waveguides to transport the signals from the scintillator WLS fibers. The readout electronics and electronic calibration scheme are the same as for the liquid argon calorimeter but with adapted electronics and pulser shapes. LED systems are used as an alternate approach to calibrate the PMTs.

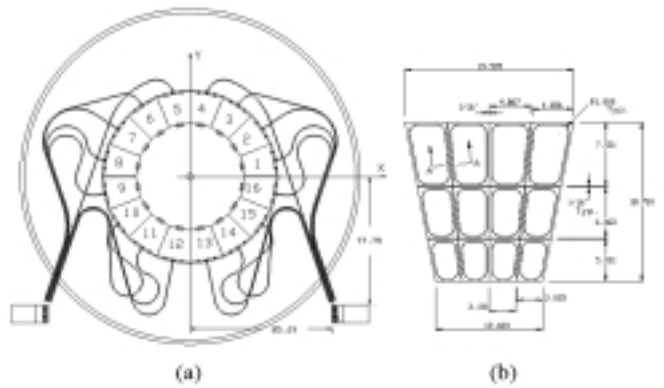


Fig. 4. (a) Schematic of the ICD tile array hung on the inner surface of each End-cap Calorimeter cryostat, with the placement of the clear fiber

piping to the low magnetic field region. (b) Schematic of the scintillator within one ICD tile module. Straight lines indicate the isolation grooves. Wavelength shifting fibers are placed in the curved grooves.

B. Upgraded Calorimeter Electronics

To accommodate the Run II bunch spacing time, and to maintain the Run I noise performance, newly designed calorimeter electronics [4] is necessary. The noise is the sum of electronic, uranium and pile-up contributions. It is necessary to optimize the relative noise contributions and to add analog storage device on which the calorimeter signals can be stored until a L1 trigger decision be made. This also requires a new strategy for the baseline subtraction.

A schematic diagram of the Run II calorimeter readout chain is shown in Fig. 5. To minimize the sensitivity to reflections, new impedance-matched $30\ \Omega$ signal cables replaced the former $110\ \Omega$ cables between the detector and the low-noise preamplifiers for a total of about 55,000 channels. The replacement cable lengths are also tuned for faster charge collection and individual channel timing equalization.

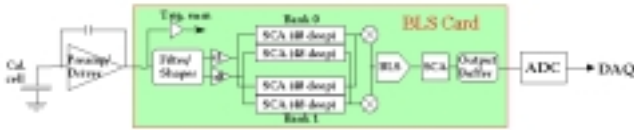


Fig. 5. Readout chain of the calorimeter in Run II.

The new charge-integrating preamplifier (preamp) is a hybrid circuit on ceramic, similar to the Run I version. Two input low-noise jFETs in parallel are used to compensate for the higher electronic thermal noise due to the shorter shaping time. Output driver stages are added for terminated signal transmission and to provide current drive and differential output capability. To make the preamplifier output waveform as similar as possible for all channels, fourteen (and additional one for ICD) different species of preamplifiers are used to compensate for various capacitances of detector cells. Forty-eight preamplifier hybrids are socket mounted on a single preamplifier motherboard that connects to the backplane of a preamplifier box on the top of the calorimeter cryostat. Each box houses 96 preamplifier motherboards and are powered by low-noise commercial switching 2 kW power supplies, which are located in steel boxes to shield the residual magnetic field of 300 gauss. Calibration pulses are injected to preamplifiers through 0.1% precision resistors.

Signals from the preamplifiers are driven through $115\ \Omega$ twist and flat cables of about 25 m in length to the Baseline Subtractor (BLS) boards which sit in crates on the platform underneath the detector. One BLS board contains 4×12 signal shapers, trigger pick-off and summation circuits, 4 BLS daughtercards, and output drivers to the ADCs. One BLS daughtercard holds 5 Switch Capacitor Array (SCA) chips, each of which contains a 12-channel by 48-depth capacitor array to pipeline the analog signals. Four of the SCA chips (L1

SCAs) store the signals until a L1 trigger decision can be made $4.2\ \mu\text{s}$ later. The SCA is not designed for simultaneous reading and writing, so two SCAs are used for the same channel so that one can be read out while the other is being written. The SCA can store analog voltages from 0-5 V in level with a precision greater than 12 digital bits. In order to achieve a 15-bit dynamic range, the shaped signals are passed through two different gain paths ($\times 1$ and $\times 8$), where the signals are simultaneously sampled and stored into two parallel SCAs. So a total of 4 L1 analog buffers are used for every channel. This provides a deadtimeless operation for a L1 trigger rate up to 10 kHz. If the L1 trigger system accepts the event, a *baseline subtraction* is performed and the result is sent to a fifth SCA (L2 SCA) at the same depth as the L1 pipeline, where it awaits a L2 trigger decision. After the L2 trigger acceptance is received, the signal is read out from the appropriate depth in the L2 SCA and sent to the ADCs (Analog to Digital Converters), which digitize and zero-suppress the signals, and then send them to the Data Acquisition System (DAQ). The ADCs have only a 12-bit dynamic range, but a low and high gain path for each readout channel ($\times 1$ and $\times 8$) maintain the 15-bit dynamic range. This matches the measured accuracy of the SCA.

The shaped signals are sampled every 132 ns, and pipelined in L1 SCAs for storage. The timing is tuned such that the shaped output can be sampled at its peak at about 320 ns. Because of this earlier sampling time compared to the liquid argon drift time of 430 ns, only 2/3 of the charge in the detector is used to form the preamplifier signal. The preamplifier output is an integral of the detector signal characterized by a rise time of about 430 ns and a recovery time of 15 μs . In order to remove slowly varying offsets and the pileup of events from neighboring bunch crossings, the pulse height sampled 396 ns earlier is used as the baseline, and then subtracted from the current pulse height. This process is called the baseline subtraction.

A fast trigger pickoff signal for each channel is obtained by a hard RC differentiation of the preamplifier output by the shaper hybrid. The calorimeter L1 trigger uses the energy summed in trigger towers of size 0.2×0.2 in $\Delta\eta \times \Delta\phi$ by trigger summers. Coordination between the trigger framework and the calorimeter readout is done by the new timing and control system. It receives trigger, accelerator and clock information through the serial command link and provides information of the appropriate locations in the pipelines to be readout at each trigger level. The timing and control is performed by the FPGA (Field Programmable Gate Array) chips.

C. Calorimeter Calibration System

The calorimeter calibration system [5] consists of twelve identical units used for the liquid argon calorimeter and one slightly modified unit for the ICD. Each unit is composed of one pulser control board and its power supply, located in the

BLS racks on the detector platform, and six active Fanout boards, housed inside of the preamplifier boxes on the cryostats. The pulser control boards are programmed via a serial bus to a VME I/O register, which can set the amplitude and the delay of the calibration signal and select the channels to be pulsed. The pulser control board delivers both a DC current corresponding to the chosen pulse height for each selected channel and a differential ECL command signal to the Fanout boards. The pulse heights are set through a 18-bit DAC, with a 100 mA maximum current delivered, and the delays are set through six programmable 8-bit delay lines with a step of size about 2 ns. There are sixteen switches located on each Fanout board. On the reception of a command, the switch converts the DC current to calibration pulse and delivers 2 calibration signals. Each calibration signal is sent to 4 preamplifier boards, hitting 6 preamplifiers on each board. Thus, one pulser talks simultaneously to 48 preamplifiers.

IV. CALORIMETER CALIBRATION

The installation and commissioning of the new calorimeter electronics was complete. A variety of measurements and studies have been done and some are still ongoing for various respects of the calorimeter calibration. Here we only give an overview of some selected online and offline calibrations.

A. Online Calibration

In the calorimeter calibration system, both the pulser control board and the Fanout board have been tested and shown to provide a pulser signal with deviations from linearity within 0.1%. After the final installation all the pulse shapes have been measured to estimate the systematic effects on the signal amplitude, the timing and the charge injected. The purity of the liquid argon is critical to the detector performance on energy measurement. We have measured the liquid argon impurity to be less than 0.15 ppm, which is less than the 0.5 ppm specification.

At the beginning of the commissioning we checked the continuity of the cables from the calorimeter cells inside the cryostat to the preamplifiers, by injecting a step pulse and measuring the reflected pulse from the calorimeter cells. The reflected pulse shape can be modeled using appropriate detector capacitances and cable impedances. We have found less than 0.05% of the cables have problems that can not be repaired. These bad cables are randomly distributed, thus have minimal impact on the calorimeter data. We regularly debug the entire readout chain by checking the mean values of pedestals and the noise for every channel, as well as the response of every channel to the injected calibration pulses. Efforts are made to fix bad channels and maintain the percentage of bad channels within 0.1%, which are also randomly distributed over the entire detector and are suppressed during data taking. Other detailed debugging includes checking the variation of the signals stored at all depths in the pipeline of SCAs, monitoring the stability of the

pedestals over time, etc. The correlated noises within calorimeter readout channels, as well as those introduced by other detector systems (e.g., tracking system) are being studied.

We tuned the timing to sample the shaped calorimeter signal at its peak. The timing measurement was done by taking 3 samples of the same signal, with the nominal peak sample taken at the point defined by the trigger, an early sample taken 132 ns earlier and a late one 132 ns later. By comparing the ratios of these three samples with a simulated model, we can accurately determine the nominal sampling position with respect to the shaped signal peak. We have measured the channel-to-channel variation of the nominal sampling time is less than 10 ns, which implies less than 0.1% variation in the peak sampled value due to timing differences.

The linearity of the calorimeter electronics and the pulser system is verified by a comparison of the electronics response versus the pulse height for each gain path ($\times 1$ and $\times 8$). We have measured excellent linearity for calorimeter energy deposits greater than 1 GeV, where the non-linearity is found to be $< 0.3\%$. For smaller energies the non-linearity is non-negligible and has been traced back to the SCAs. We use a parameterized function to correct the non-linearity, with the parameters adjusted for all channels. We have further compared the linearity from two calibration runs taken one year apart, and the agreement between them shows the stability of the electronics.

B. Offline Calibration

We keep online monitoring the calorimeter data quality (energy distribution, channel occupancy, trigger rate, noisy cells, etc.) during the data taking. Analyzing the offline data for physics studies also gives feedbacks on the calorimeter performance, both at the cell energy level and at the reconstructed particle level. Such feedbacks are especially useful on subtle problems which may not be revealed by online calibration. Some noisy calorimeter L1 trigger towers and trigger cabling problems have been traced and fixed. A ϕ inter-calibration has been performed to calibrate the uniformity of the calorimeter response in ϕ from 0 to 2π . This takes into account the variations between the different calorimeter modules due to the inhomogeneous distributions of non-instrumented materials in front of the cryostats.

We calibrate the calorimeter EM energy scale (for electron and photon) from the reconstructed events of Z^0 resonance. The absolute energy scale is obtained by reconstructing the mass of the Z^0 resonance from its decay product of two electrons, and adjusting the value to the LEP measured Z^0 mass value (about 91 GeV/c²). The comparison of E/p is obtained using the reconstructed events of W decaying into an electron and an electron neutrino, with the electron energy measured by calorimeter and its momentum measured by tracking system. The EM energy scale at low energy is calibrated using J/ ψ (mass around 3.1 GeV/c²) and Y (mass around 9.5 GeV/c²) events. QCD events are used to calibrate the calorimeter

response to the hadronic jets. The measurement of the missing transverse energy, obtained by summing up the transverse energies of all cells as vectors, is also a good check on the calorimeter performance.

The calorimeter response to jets is crucial to determine the jet energy scale. For most measurements on jets, the response of the jet should be known at the particle level and be corrected for all detector effects. To determine the calorimeter response of jets, γ -jet events are selected and the transverse energy of the jet is compared to the calibrated energy of the photon (the calorimeter response to photon is exactly the same as to electron). The response function obtained for a cone-algorithm jet is shown in Fig. 6. A new jet algorithm, the energy flow algorithm, has been recently developed. Based on the cell-nearest-neighbor clustering, this algorithm further combines the information from both the calorimeter and the tracking system to improve the jet energy resolution. The current performance of the energy flow algorithm is comparable with the standard cone algorithm on Monte Carlo jets. Studies are going on to improve this algorithm and to apply it on data.

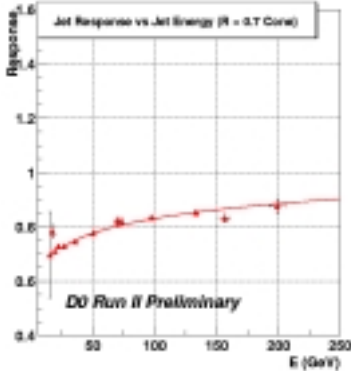


Fig. 6. Response function of jets compared to photons.

V. PHYSICS STUDIES

Physics analyses using Run II calorimeter data have been actively performed at DØ. Preliminary results of QCD, electroweak, B, Higgs, top and new phenomena physics have been shown on various conferences. For example, Fig. 7 plots the inclusive jet cross section as a function of the jet transverse energy, with the measured values compared to the theoretical predictions of perturbative QCD. The jet energies are corrected using the jet energy scale obtained from Run II calorimeter data. As another example, the cross section of Z^0 was measured in the di-electron decay channel. The distribution of the invariant mass of the two electrons for Z^0 candidates is shown in Fig. 8 (QCD background has been subtracted). The Z^0 mass peaks at 91 GeV/c² on the plot. The cross section times branching ratio of Z^0 is measured to be:

$$\sigma_Z \times \text{Br}(Z \rightarrow e^+e^-) = 275 \pm 9 \text{ (stat.)} \pm 9 \text{ (syst.)} \pm 28 \text{ (lumi.) pb}$$

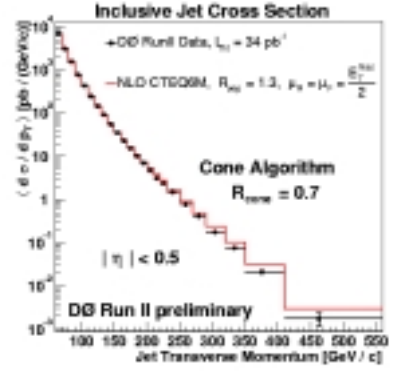


Fig. 7. The inclusive jet cross section as a function of the jet transverse energy. The data are compared to the theoretical predictions of perturbative QCD in NLO (next-to-leading order).

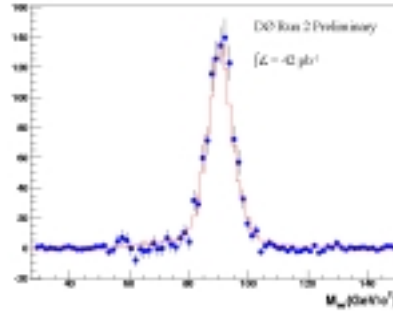


Fig. 8. The invariant mass distribution for Z^0 candidate events in the di-electron decay channel. The points show the background-subtracted data and the histogram shows the Monte Carlo.

VI. CONCLUSION

We have finished commissioning of the new calorimeter electronics, and performed online and offline calibrations. The new calorimeter electronics has been performing well in data taking. Physics analyses using the calorimeter data are undergoing and preliminary results have been shown. We will study the calibrations in more details to better understand the data and to improve the physics results.

VII. ACKNOWLEDGMENT

Thanks to all the colleagues in the DØ calorimeter group.

VIII. REFERENCES

- [1] R. D. Schamberger, "The DØ calorimeter performance and calibration," in *Proc. fifth Calorimetry in High Energy Physics*, H. Gordon and D. Rueger, Upton, NY: World Scientific, 1994, pp. 39-50.
- [2] The DØ Collaboration, S. Abachi et al., "The DØ detector," *Nucl. Instrum. Methods Phys. Res.*, A 338, p. 185, 1994.
- [3] L. Sawyer et al., "Technical design report for the upgrade of the ICD for DØ Run II," Internal DØ-note 2686, 1997.
- [4] A. Kotwal et al., "Calorimeter electronics upgrade for Run II: Technical design report," Internal DØ-note, 1998.
- [5] P. Corneise et al., "Run II calorimeter calibration system," Internal DØ-note 3731, 2000.